ADVANCED ENERGY & SUSTAINABILITY RESEARCH
Open Access
www.advenergysustres.com

Electrode Engineering Study Toward High-Energy-Density Sodium-Ion Battery Fabrication

Toshihiko Mandai, Umi Tanaka, and Shin Kimura*

Sodium-ion batteries (SIBs) are emerging as promising energy storage technologies, particularly for grid-scale applications, due to their low material costs stemming from abundant natural resources. Meeting the increasing demand for higher energy density requires the development of innovative electrode and electrolyte materials, along with advanced analytical and fabrication techniques. However, the energy density of SIBs is often evaluated based solely on the capacities and cell voltages of active materials in half-cell configurations, neglecting engineering considerations for full-cell configurations. This study investigates the effects of electrode composition and the balance in capacities between positive and negative electrodes (N/P ratio) on the performance of full-cell configurations, using $Na_3V_2(PO_4)_3$ (NVP) and hard carbon (HC) as representative electrode materials. Through a systematic analysis, an optimal composition for NVP and HC electrodes is proposed, considering areal capacity and capacity retention during full-cell operations. Additionally, the importance of balancing the N/P ratio and the necessity of presodiation techniques to achieve high-energy-density SIBs are underscored. Overall, this work sheds light on key factors influencing the performance of SIBs and provides insights into strategies for enhancing their energy density and operational efficiency.

1. Introduction

Electrochemical energy storage technologies, such as lithium-ion batteries (LIBs), have rapidly evolved alongside industrial and technological advancements, becoming indispensable devices in our daily lives. However, this progress has been accompanied by environmental challenges, including global warming, stemming from the recent industrial revolution. To mitigate environmental degradation and foster a sustainable future society, there is a pressing need to transition from current technologies and further innovate in energy storage.

Lithium, a crucial component in LIB manufacturing, is often considered a scarce mineral resource. However, based on current battery production scales, estimates suggest that lithium resources on Earth are abundant enough to last over 200 years[1] without depletion. Therefore, lithium resources themselves are not expected to pose a significant bottleneck in large-scale battery production. Nonetheless, concerns persist regarding stable supply and costs due to resource concentration in specific regions. Moreover, the process of converting lithium raw materials containing LiCl and Li_2CO_3 into metal resources, essential for battery production, generates substantial CO_2 emissions and waste,[2] highlighting the urgent need to reduce environmental impacts. Against this backdrop, the development of energy storage technologies utilizing resources unaffected by constraints and with minimal environmental footprints is eagerly anticipated.

Sodium-ion batteries (SIBs) are promising energy storage technologies for auxiliary power supply in electric devices and grid-scale applications, thanks to their relatively wide operating temperature range and low material costs due to the abundance of sodium resources.[3,4] Extensive research has been conducted on electrode and electrolyte materials to achieve SIBs with competitive or superior performance compared to current LIBs. Despite the challenges inherent in surpassing LIBs' energy storage performance with SIBs, specific materials tailored for sodium-ion storage have been developed with the help of advanced characterization techniques and computational science.[5–8] However, the energy density of SIBs is often evaluated based solely on the capacities and voltages of active materials in half-cell configurations, disregarding practical considerations for full-cell configurations and engineering aspects. Limited

T. Mandai
Functional Electrolyte Synthesis Team
Research Center for Energy and Environmental Materials
National Institute for Materials Science (NIMS)
1-1 Namiki, Tsukuba, Ibaraki 305-0044, Japan
E-mail: MANDAI.Toshihiko@nims.go.jp

T. Mandai, U. Tanaka
Center for Advanced Battery Collaboration
Research Center for Energy and Environmental Materials
National Institute for Materials Science (NIMS)
1-1 Namiki, Tsukuba, Ibaraki 305-0044, Japan

S. Kimura
Battery Research Platform
Research Center for Energy and Environmental Materials
National Institute for Materials Science (NIMS)
1-1 Namiki, Tsukuba, Ibaraki 305-0044, Japan

The ORCID identification number(s) for the author(s) of this article can be found under https://doi.org/10.1002/aesr.202400059.

DOI: 10.1002/aesr.202400059

reports exist on the engineering aspects of fabricating SIB full cells, such as experimental conditions for slurry preparation,[9,10] loading amounts of active materials,[11,12] and balancing capacities between positive and negative electrodes (N/P ratio).[13,14] This oversight can lead to an overestimation of SIBs' potential.

This study systematically investigates the effects of electrode composition and the N/P ratio on the energy storage performance of full-cell configurations, using $Na_3V_2(PO_4)_3$ (NVP) and hard carbon (HC) as positive and negative electrodes, respectively, aided by an energy density calculator. The results of the systematic survey using model systems confirm that careful balancing of the N/P ratio is crucial for enhancing the energy density of SIBs. Additionally, two presodiation approaches are adopted to fabricate SIB full cells with a 100 Wh kg^{-1} energy density class, mitigating unbalanced N/P ratios resulting from the consumption of reactive Na^+ during initial stabilization processes.

2. Results and Discussions

2.1. Binder, Conductive Support, and Electrolyte Study on Half-Cell Configuration

Various binder polymers are utilized in the production of composite electrodes, taking into account factors such as cost-effectiveness, eco-friendliness, processability, and battery performance. The physical properties of binder polymers significantly impact the resulting battery performance. Polyvinylidene difluoride (PVdF), a fluorocarbon-based polymer, is widely used, particularly for positive electrodes in commercial LIBs, due to its numerous advantageous properties.[15] Given its adhesiveness and excellent electrochemical stability, PVdF was chosen as the binder polymer for the NVP electrodes in this study. **Figure 1** illustrates the typical charge–discharge profiles of [Na | base electrolyte | NVP] half cells employing low (L) and high (H) molecular weight PVdF, L-PVdF and H-PVdF, polymers as binders. The composite working electrodes consisted of NVP, acetylene black (AB), and PVdF in a weight ratio of 85:5:10. These two composite NVP electrodes are subsequently referred to as $NVP_{AB/L\text{-}PVdF}$ and $NVP_{AB/H\text{-}PVdF}$. As depicted in Figure 1, the choice of binder significantly affects the charge–discharge performance. $NVP_{AB/H\text{-}PVdF}$ exhibited higher reversible capacities over 100 cycles, while capacities rapidly decreased for $NVP_{AB/L\text{-}PVdF}$. A similar trend was observed for comparative [Na || NVP] cells using relatively coarse NVP particles and different electrolytes (Figure S3, Supporting Information).

To comprehend the potential causes of the observed differences with different binders, the physical structure of the composite electrodes was analyzed via scanning electron microscopy (SEM). Unfortunately, it was challenging to identify decisive differences in their physical structure, as depicted in **Figure 2**. It can be inferred that, concerning homogeneity, the active materials and conductive carbons are relatively well homogenized for $NVP_{AB/H\text{-}PVdF}$, whereas these components are somewhat aggregated in parts for $NVP_{AB/L\text{-}PVdF}$. Such aggregation may impede electron and ion conduction in the composite electrodes, potentially leading to inferior charge–discharge performance. Due to the superior performance of electrodes with H-PVdF,

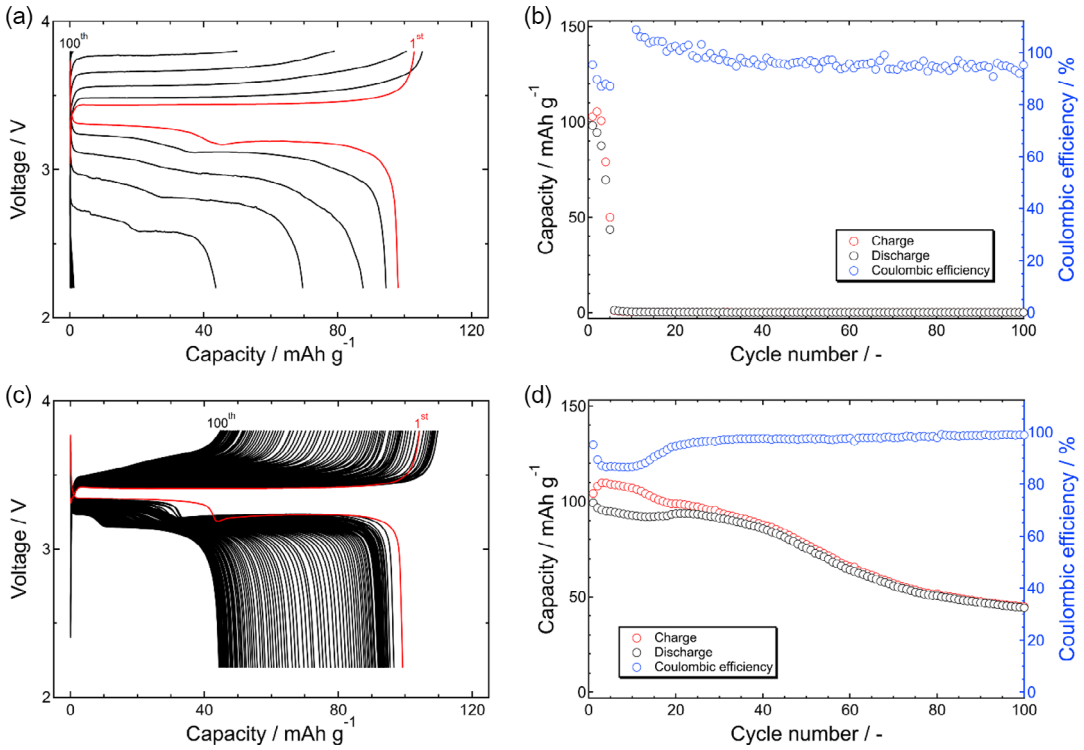

Figure 1. a,b) Galvanostatic charge–discharge cycling profiles and the corresponding Coulombic efficiency of [Na || NVP] half cells employing $NVP_{AB/L\text{-}PVdF}$ and c,d) $NVP_{AB/H\text{-}PVdF}$ electrodes.

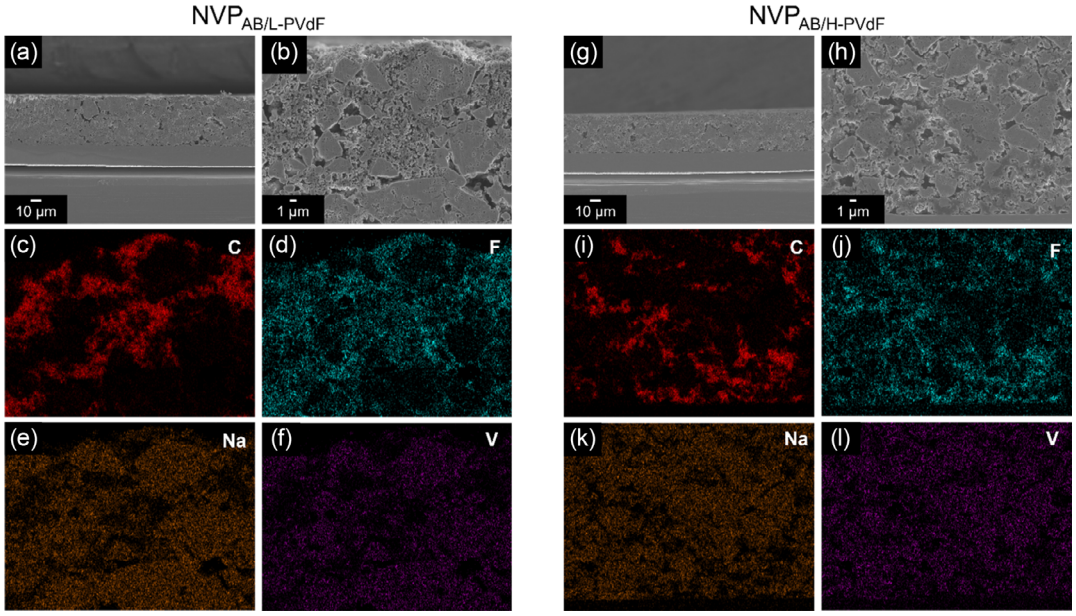

Figure 2. a–f) Cross-sectional SEM images and corresponding EDX mapping profiles of $NVP_{AB/L-PVdF}$ and g–l) $NVP_{AB/H-PVdF}$ electrodes.

all subsequent studies utilized this binder for the NVP electrodes, unless otherwise specified.

The impact of conductive support on enhancing the energy storage performance of electrodes was investigated in this study. By partially replacing AB with carbon nanotube (CNT), the relative amount of PVdF binder could be significantly reduced, resulting in NVP electrodes ($NVP_{CNT/H-PVdF}$) with a weight ratio of NVP:carbon:binder = 92:4:4. These electrodes exhibited comparable performance to those containing higher amounts of binder (**Figure** 1b and **3**), attributed to the fiber properties of CNT facilitating the folding of active materials. Additionally, spaces between NVP particles were observed in $NVP_{CNT/H-PVdF}$ (Figure 3), likely contributing to enhanced penetration of electrolyte solutions throughout the composite electrodes. This positively affected electrode performance by improving ion transport characteristics. Fabricating electrodes with higher relative content of active materials and lower content of other components is beneficial for achieving energy and power-balanced batteries, avoiding thick electrodes due to excessive amounts of conductive supports and binders.

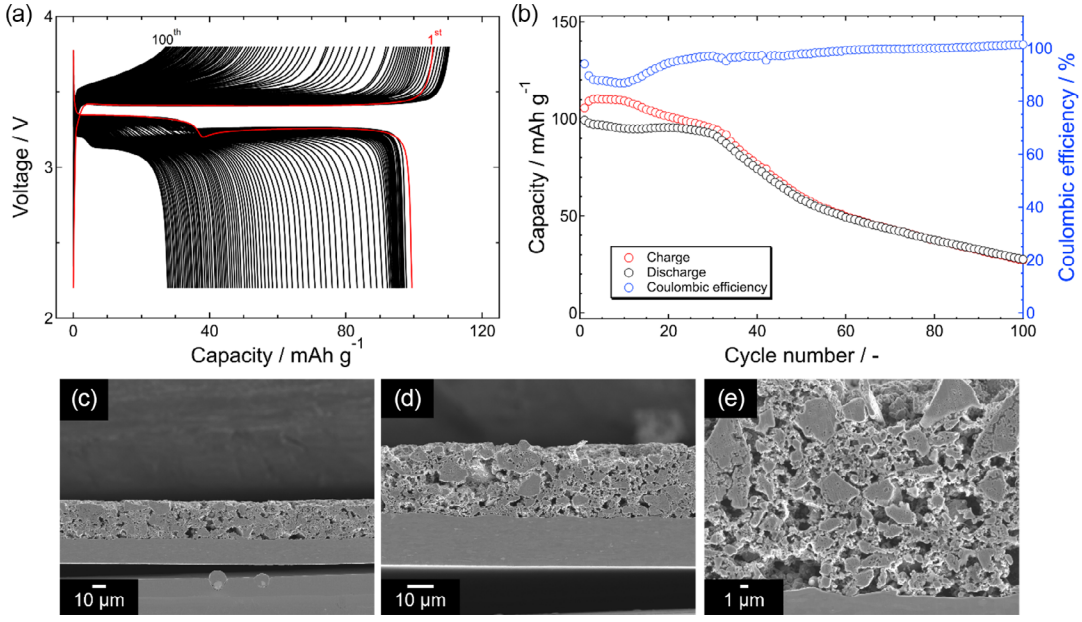

Figure 3. a) Galvanostatic charge–discharge cycling profiles and b) the corresponding Coulombic efficiency of [Na || NVP] half cell employing a $NVP_{CNT/H-PVdF}$ electrode. c–e) Cross-sectional SEM images of $NVP_{CNT/H-PVdF}$ electrodes.

For hard carbon (HC)-negative electrodes, aqueous mixtures of carboxymethyl cellulose (CMC) and styrene-butadiene rubber (SBR) are commonly used to create composite electrodes. In these mixtures, SBR acts as a binder while CMC serves as a thickener to regulate slurry viscosity.[15] Similar to graphite electrodes in LIBs, a conductive support is necessary for HC electrodes, possibly due to the insufficient electronic conductivity of HC powder itself. HC electrodes without AB ($HC_{AB\text{-}free}$) did not perform well in [Na || HC] cells, whereas those incorporating AB exhibited some reversible capacities, as shown in **Figure 4** and S4a, Supporting Information, respectively. The effect of binder composition in HC-negative electrodes was also examined. Although some activation process is necessary, and the initial deliverable capacities after the activation process are inferior for HC electrodes containing 3 wt% of CMC-SBR mixture ($HC_{3\%CMC\text{-}SBR}$) compared to those with 5 wt% ($HC_{5\%CMC\text{-}SBR}$), the former electrodes demonstrated better capacity retention over 100 cycles (Figure 4).

The systematic comparative experiments clearly reveal the electrolyte-dependent charge–discharge characteristics of [Na || HC] and [Na || NVP] half cells. The [Na || HC] half cells utilizing the carbonate-based base electrolyte exhibited unexpectedly low capacities (Figure 4). Previous reports on the sodiation mechanism of HC indicate that the slope region in the charging profiles, ≈1.0–0.2 V versus Na^+/Na, is attributed to surface adsorption and/or intercalation of Na^+ on/into the defective HC structure, while the plateau region around 0.02–0.01 V versus Na^+/Na arises from clustering of Na(0) in (pseudo-)closed pores.[16,17] Based on this mechanism, the observed results with the base electrolyte suggest no or limited Na(0) clustering. Conversely, cells with the ether-based counterpart, $NaPF_6$/G2 (G2; diglyme), delivered reasonable HC capacities (≈240 mAh g^{-1}) under the same experimental conditions, albeit with irregularly fluctuating profiles presumably due to microshorts (Figure S5, Supporting Information). The reductive stability of the solvents in these electrolytes may explain the observed differences. Carbonates are known to be susceptible to reduction, leading to successive decomposition of carbonate molecules upon contact with highly reductive Na metal during charge–discharge cycling. Additionally, stable solid electrolyte interface (SEI) formation on the surface of Na metal is challenging in conventional carbonate-based electrolytes.[18,19] This unstable interface can cause significant polarization of Na plating/stripping at Na metal counter electrodes, resulting in limited or no utilization of micropores for Na(0) accommodation in HC electrodes. While micropores can be utilized for Na^+ accommodation by adjusting the experimental cut-off potential, changing the potential from +0.01 to −0.05 V versus Na metal may increase the risk of short-circuit due to Na metal deposition on the surface of HC electrodes (Figure S6, Supporting Information). In contrast, stable Na plating/stripping is reportedly possible in ether-based electrolytes due to their greater stability against Na metal.[20,21] This enhanced stability contributes to the relatively stable cycling of [Na || HC] cells (Figure S5, Supporting Information). The stability of the electrolyte against Na metal counter electrodes also significantly affects the observed performances of [Na || NVP] cells (Figure 1 and S3, Supporting Information). It is important to note that ethereal solvents are incompatible with most positive electrodes of SIBs due to their anodic limits lying around 3.8 V versus Na.[22] The charge curves

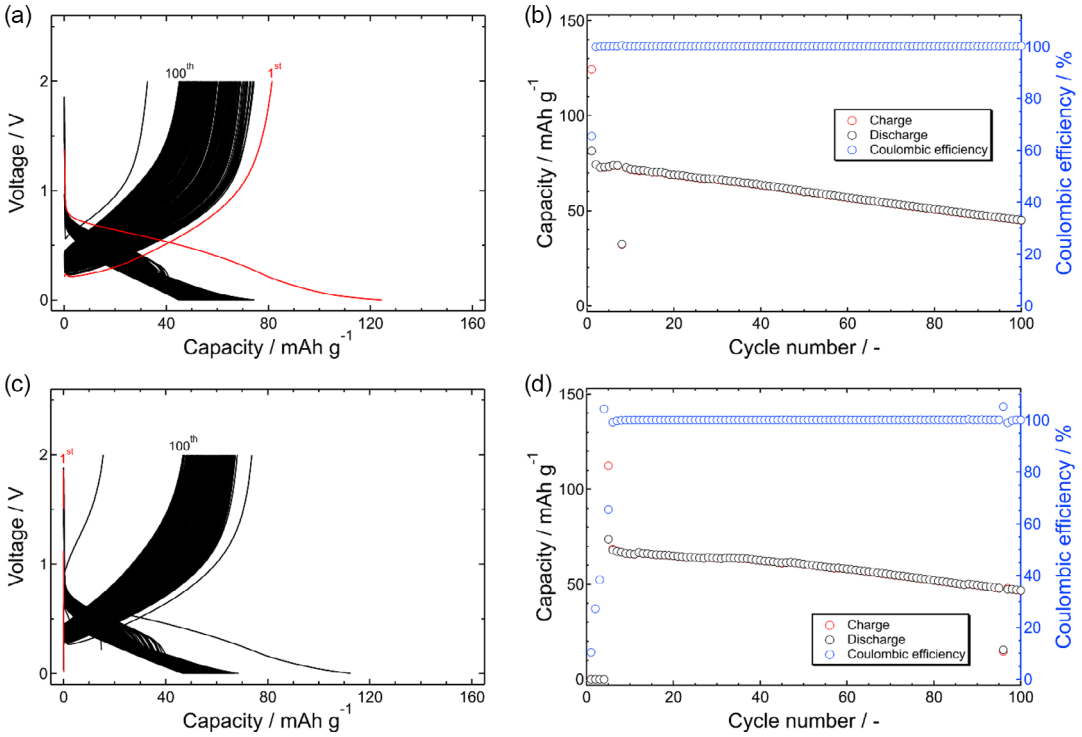

Figure 4. a,b) Galvanostatic charge–discharge cycling profiles and the corresponding Coulombic efficiency of [Na || HC] half cells employing $HC_{5\%CMC\text{-}SBR}$ and c,d) $HC_{3\%CMC\text{-}SBR}$ electrodes.

of [Na || $NVP_{CNT/H\text{-}PVdF}$] cells with the $NaPF_6$/G2 electrolyte indeed indicate electrolyte decomposition associated with charging (Figure S3, Supporting Information).

In summary, comprehensive studies on the half-cell configuration can provide guidance for the favorable composition of composite electrodes. However, the incompatibility of electrolytes against Na metal counter electrodes can lead to misconceptions regarding the obtained experimental results. Fluoroethylene carbonate (FEC) is well-known as an SEI-forming additive for electrode materials, including carbonous and metallic negative electrodes. The incorporation of FEC in typical $NaPF_6$/carbonate-based electrolytes can significantly enhance Na plating/stripping efficiencies.[23] The integration of FEC is somewhat effective in enhancing the cycling stability of [Na || $NVP_{CNT/H\text{-}PVdF}$] half cells (Figure S7, Supporting Information). Unfortunately, the integration of FEC also results in fluctuations in charge–discharge performance, possibly due to the crossover of decomposition products. To further optimize both NVP and HC electrodes without the contribution of ambiguous impurities and relevant misconceptions arising from electrolyte additives, the electrochemical performances will be studied under the full-cell configuration with carbonate-based base electrolytes.

2.2. Full-Cell Fabrication and Optimization of Composite Electrodes

The battery performance of the primary full cells, [HC || NVP], was evaluated using coin-type cells. **Figure 5** summarizes the charge–discharge cycling profiles of the full cells with three different compositions in composite electrodes. To minimize the influence of the balance in capacities of the positive and negative electrodes, the N/P ratio was fixed at ≈1.70–1.73 among the cells. Similar to the performance of the corresponding half cells described above, the composition of each positive and negative electrode significantly impacts the full cell performance. Regarding the positive electrodes, the cells with the optimal $NVP_{CNT/H\text{-}PVdF}$ electrodes showed superior capacities from both gravimetric and areal perspectives. These results further demonstrate the beneficial effect of CNT on enhancing the energy density of batteries. Conversely, the absence of AB in HC electrodes resulted in significantly inferior performance. It is worth noting that the corresponding half cells did not function at all (Figure S4, Supporting Information). This discrepancy in the reactivity of HC electrodes may arise from the cell configuration, as relatively deep polarization during charging can activate the AB-free HC electrodes. Indeed, the charging voltage of the corresponding full cell was lower than that of the control experiment (Figure 5a,c). It is worth noting here that, as well as the cycling performance of half-cell configurations (Figure 4), the full cells using the $HC_{3\%CMC\text{-}SBR}$ showed better capacity retention than those using the $HC_{5\%CMC\text{-}SBR}$ (Figure S8, Supporting Information). Based on the results of the primary full-cell configurations, the optimal compositions of each positive and negative electrode are proposed to be NVP:carbon:binder = 92:4:4 ($NVP_{CNT/H\text{-}PVdF}$) and HC:AB:CMC-SBR = 92:5:1.5:1.5 ($HC_{3\%CMC\text{-}SBR}$), respectively. This configuration also performs well with a different electrolyte formulation (Figure S9, Supporting Information).

2.3. Factors Affecting Full-Cell Performance

It is crucial to minimize the difference in capacities between positive and negative electrodes to achieve high-energy density batteries, with the ideal N/P ratio being unity. By precisely controlling the N/P ratio, overlooked aspects for practical battery materialization, not addressed in studies on half-cell configurations, can be discussed. To avoid redundancy, the optimal electrodes mentioned earlier are hereby referred to simply as NVP and HC.

The impact of the N/P ratio on full-cell performance is evident in the cycling results of full cells with different N/P ratios, as shown in **Figure 6**. As the N/P ratio increases, initial discharge capacities decrease, although corresponding charging capacities based on the mass of NVP remain almost the same. Subsequent cycles inherit the performance of the initial cycle, with relatively inferior performance observed for full cells fabricated under higher N/P ratios. These results suggest the consumption of reactive Na^+ from the NVP cathodes by side reactions during the initial charging process. The charging capacity retention between the 1st and 2nd cycles, or simply initial Coulombic efficiency, also strongly indicates consumption of reactive Na^+ during the 1st charging. Additionally, an extra plateau around 0.8 V versus Na is observed in the initial discharge process for [Na || HC] cells (Figure 4), indicating the formation of the SEI on negative electrodes upon electrolyte decomposition.[16] Such SEI can suppress further electrolyte decomposition, thus stabilizing charge–discharge performances. Unfortunately, SEI formation consumes reactive Na^+, consequently leading to poor

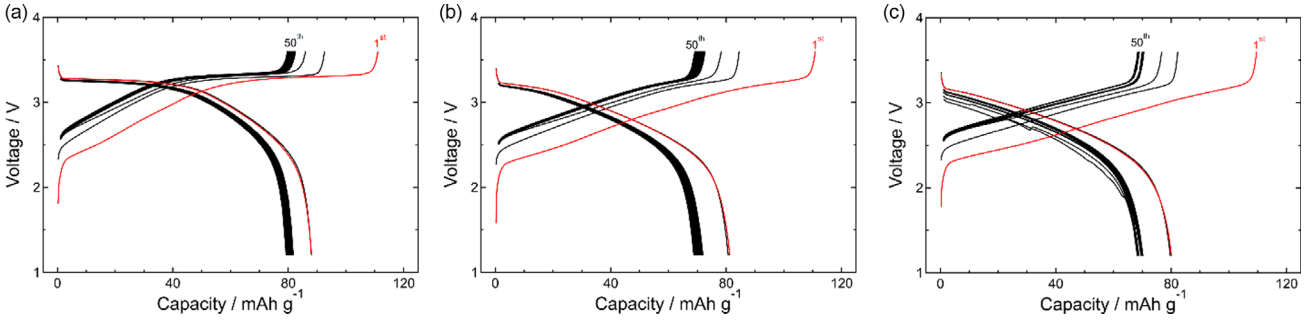

Figure 5. a) Galvanostatic charge–discharge cycling profiles of [$HC_{3\%CMC\text{-}SBR}$ || $NVP_{CNT/H\text{-}PVdF}$], b) [$HC_{3\%CMC\text{-}SBR}$ || $NVP_{AB/H\text{-}PVdF}$], and c) [$HC_{AB\text{-}free}$ || $NVP_{CNT/H\text{-}PVdF}$].

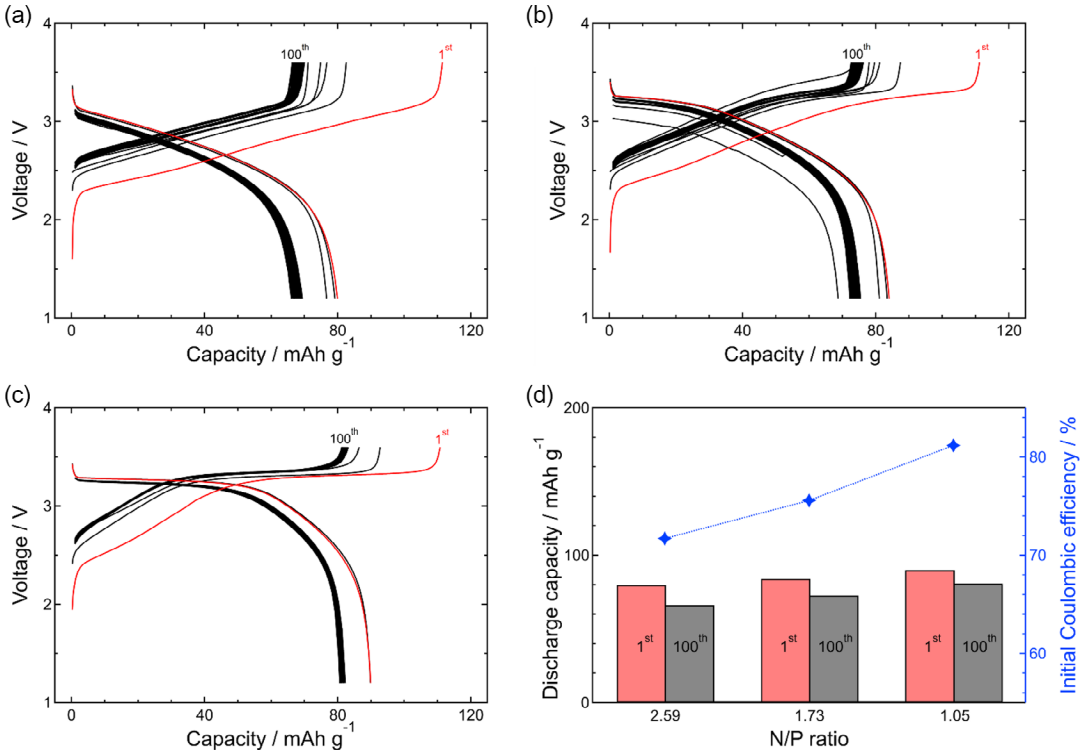

Figure 6. Galvanostatic charge–discharge cycling profiles of [HC || NVP] full cells with the N/P at a) 2.59, b) 1.73, and c) 1.05. d) Discharge capacities at 1st and 100th cycles and initial Coulombic efficiency.

energy storage performances. It is worth noting that Na metal electrodes can supply extra Na^+, making the undesired capacity decay observed in full-cell configurations difficult to observe in their half-cell counterparts. Moreover, a high N/P ratio induces sloping of the voltage plateaus during both charging and discharging, limiting the enhancement of battery energy density.

From the above results, it can be anticipated that an electrolyte additive is less effective in improving battery performance in the present case. Despite the remarkable performance improvement upon FEC integration for Na metal plating/stripping,[23] increasing the amount of electrolyte additive leads to worse cycling performance, even at the same sufficiently low N/P ratio of 1.25 (Figure S10, Supporting Information). As SEI formation associated with FEC decomposition involves the consumption of reactive Na^+ in the cells, excessive FEC additive leads to inferior performance. X-ray photoelectron spectroscopy (XPS) analysis on cycled NVP electrodes further supports the formation of thick decomposition products on the surface (Figure S11, Supporting Information). The relative peak intensity of Na–F compounds in F 1*s* spectra for HC electrodes becomes larger with the amount of the FEC additive.[24] These observations strongly suggest that the (electro)chemical stability of SEI on HC electrodes generated in the additive-free conventional base electrolytes is sufficiently high, and the reported instability of SEIs originating from conventional carbonate-based electrolytes would be induced by the crossover of harmful compounds from Na metal counter electrodes due to half-cell configurations.[18,19]

Even at minimal N/P ratios, the deliverable practical capacities of the [HC || NVP] full cells were at most ≈80 mAh g^{-1} based on the mass of NVP, corresponding to ≈70% of the theoretical capacity. Using the energy density calculator established by Ue et al.[25] the potential energy density of these full cells was calculated to be 73 Wh kg^{-1}, considering experimental parameters of composite electrodes, mass loading of NVP (≈5 mg cm^{-2}), N/P ratio (1.05), and electrolyte/capacity ratio (5.0 g Ah^{-1}). Increasing the practical capacities up to 105 mAh g^{-1} could result in an energy density of 100 Wh kg^{-1}. As the loss of capacity mainly arises from the consumption of reactive Na^+ by SEI formation during the initial charging process, presodiation was applied to compensate for the loss of Na^+. Both electrochemical and chemical presodiation were adopted in this study. Electrochemical presodiation on HC electrodes involved precharging the [HC || NVP] full cells, disassembling the cells, and reassembling them using the charged HC and fresh NVP. The N/P ratio for the precharging and subsequent charge–discharge measurements were controlled to be ≈1.1, estimated based on the mass loading and capacity of pristine electrodes. Calculations of energy density of full cells were summarized in Figure S12 and Table S1, Supporting Information.

With an increasing depth of charge for the precharging processes (DOPC), the deliverable capacities of the 1st discharge processes increased from 75 to 105 mAh g^{-1} at 0% and 100% DOPC, respectively (**Figure 7**). The charge–discharge profiles also changed with the degree of DOPC, and flat initial reaction plateaus were observed for cells precharged at 100% DOPC. However, a high degree of DOPC simultaneously led to inferior capacity retention for subsequent cycles, although the Coulombic efficiencies remained almost unity over 200 cycles, irrespective of

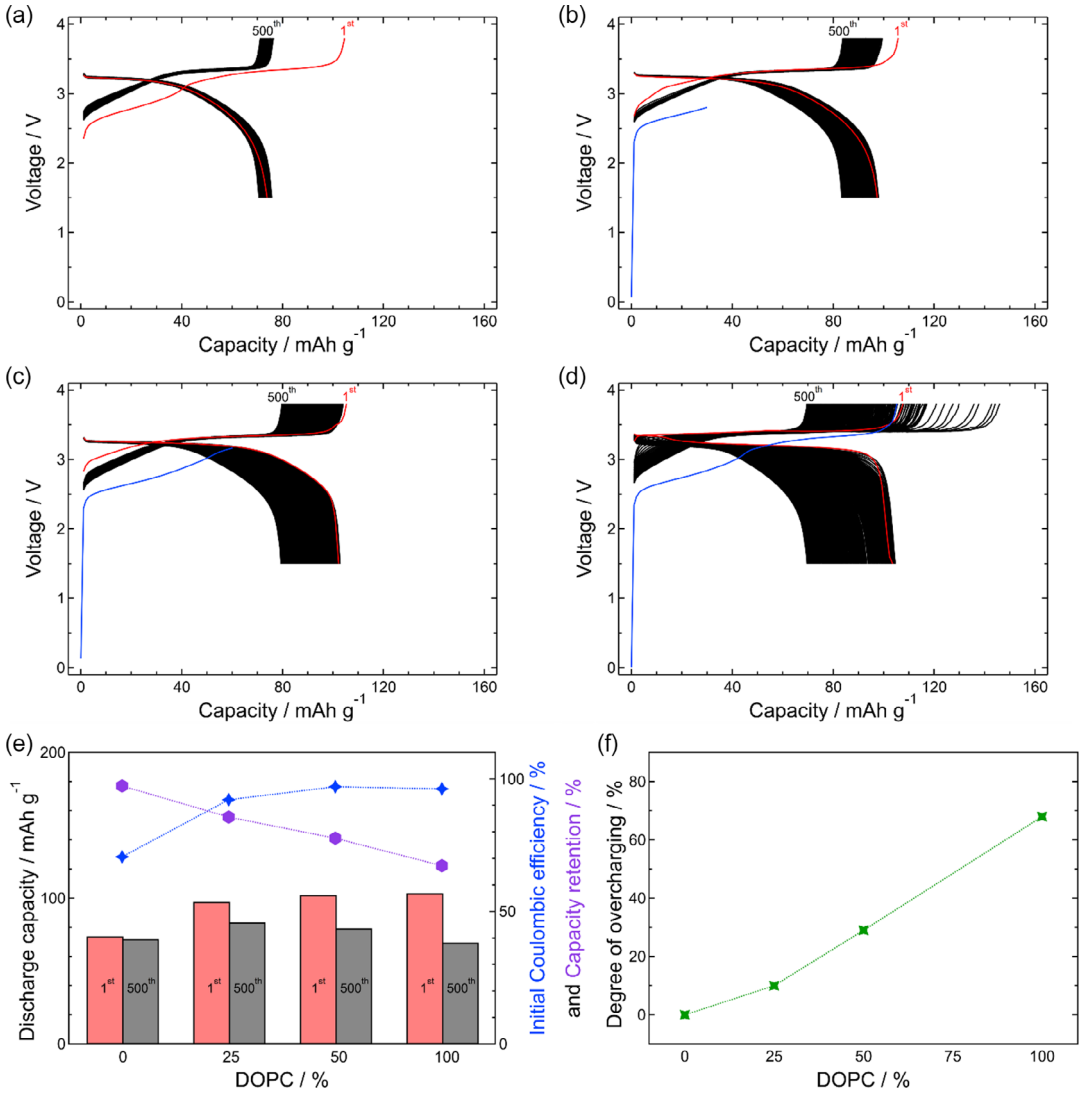

Figure 7. Galvanostatic precharging and subsequent charge–discharge cycling profiles of [HC || NVP] full cells with a different DOPC; a) 0%, b) 25%, c) 50%, and d) 100%. e) Discharge capacities at 1st and 500th cycles, initial Coulombic efficiency, and capacity retention after 500 cycles. f) Degree of overcharging of HC electrodes.

the degree of DOPC (Figure 7a–e). The capacity retention of cells precharged at 100%-DOPC was only 67.3% after 500 cycles, while those at 50%, 25%, and 0% DOPC were over 77.7%, 85.6%, and 97.4% for 500 cycles, respectively. This worse capacity retention rate for the deeply precharged cells is possibly due to the overcharging of HC electrodes and resulting in undesired side reactions, such as deterioration of the electrolyte and electrode by deposited Na metal. Based on the N/P ratios of the cells, the HC electrodes precharged at 100%, 50%, and 25% DOPC would be overcharged by ≈70%, 30%, and 10% of their practical capacity, respectively, in the following measurements (Figure 7f). The overcharged HC electrodes indeed exhibited unstable discharge–charge behavior (Figure S6, Supporting Information). To avoid such situations, the N/P ratios for both precharging and subsequent charge–discharge measurements were carefully modulated. Furthermore, to minimize the inhomogeneity in confining pressure during measurements, pouch-type cells were fabricated, and a confining pressure of 112 kPa was applied to the cells. By considering the N/P ratios, especially during subsequent charge–discharge measurements, the pouch-type [HC || NVP] full cells achieved balanced performances with respect to apparent capacities, capacity retention, and practical energy density upon modulating the N/P ratio to be 2.2, which substantially corresponds to 1.2 for the subsequent charge–discharge cycles. This primitive optimum cell showed negligible irreversible capacity between the 1st charge and discharge and delivered stable discharge capacity over 500 cycles (**Figure 8**a,b). The formation of stable SEI during the precharging process and the utilization of ≈45% of the full capacity of the precharged HC negative electrode jointly contributed to the exceptionally stable cycling performance of the present optimum cell. The practical energy density of that cell is however estimated

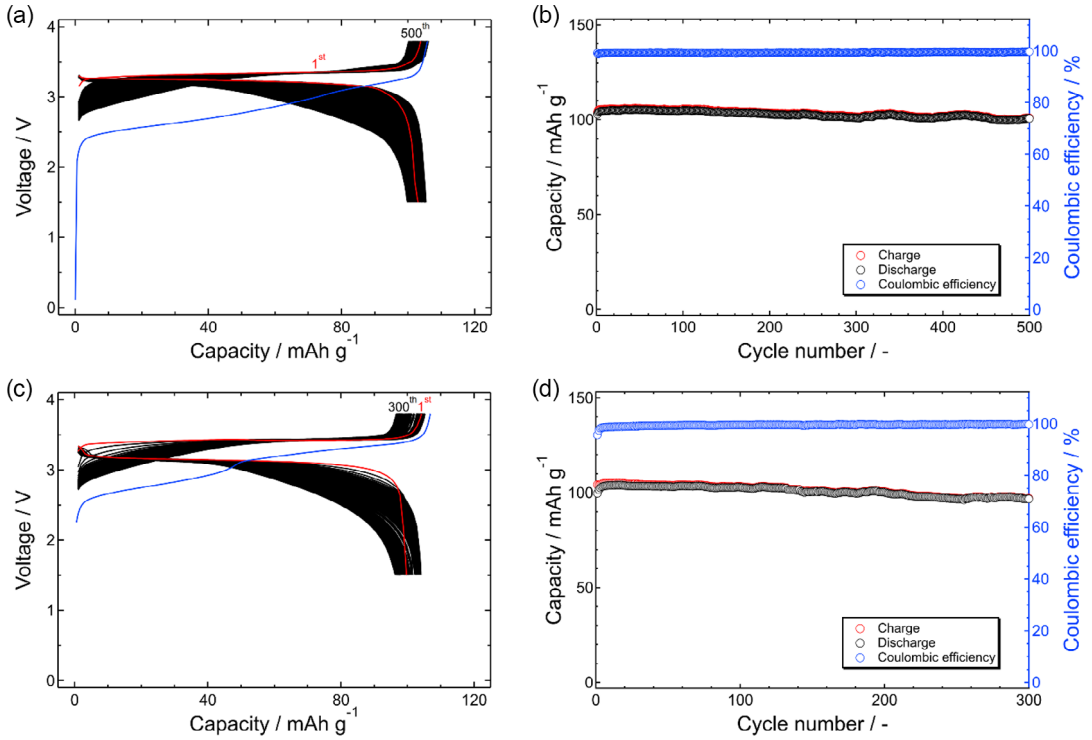

Figure 8. a,c) Galvanostatic precharging and subsequent charge–discharge cycling profiles and b,d) the corresponding Coulombic efficiency of pouch-type [HC || NVP] full cells. Mass loading of NVP; (a,b) 5 mg cm^{-2}; (c,d) 11 mg cm^{-2}.

to be 85 Wh kg^{-1}, still less than 100 Wh kg^{-1}, certainly due to a relatively high N/P ratio (Figure S12 and Table S1, Supporting Information). The significant loss in the energy density was compensated by other engineering approaches. Upon increasing the mass loading of the electrodes, from 5 to 11 mg cm^{-2} for NVP, the resulting energy density can reach 105 Wh kg^{-1} even at the N/P ratio of 2 (Figure S12 and Table S1, Supporting Information). The stable charge–discharge performance of the well-designated pouch-type cell has successfully been demonstrated (Figure 8c,d).

Although electrochemical presodiation can give significant insights for full-cell fabrication, this method complicates the manufacturing of SIBs, leading to high production costs, thus is unadoptable to practical operation. The present systems also require a relatively high N/P ratio to stabilize HC electrodes. Decreasing the N/P ratio from 2.2 to 1.05 in the same [HC || NVP] setup can increase the energy density to 120 Wh kg^{-1}. Chemical presodiation and/or inclusion of sacrificial additives have been proposed as alternatives.[26–29] Chemical presodiation on HC electrodes can lead to instability of the resulting electrodes against the ambient atmosphere due to the accommodation of reactive Na^+ and Na(0) species in their structure.[28,29] Conversely, chemical presodiation on NVP cathodes is expected to be more accessible owing to the potential chemical stability of the presodiated NVP, $Na_4V_2(PO_4)_3$.[26] The chemically-sodiated NVP coupled with HC electrodes at N/P = 1.2 showed an

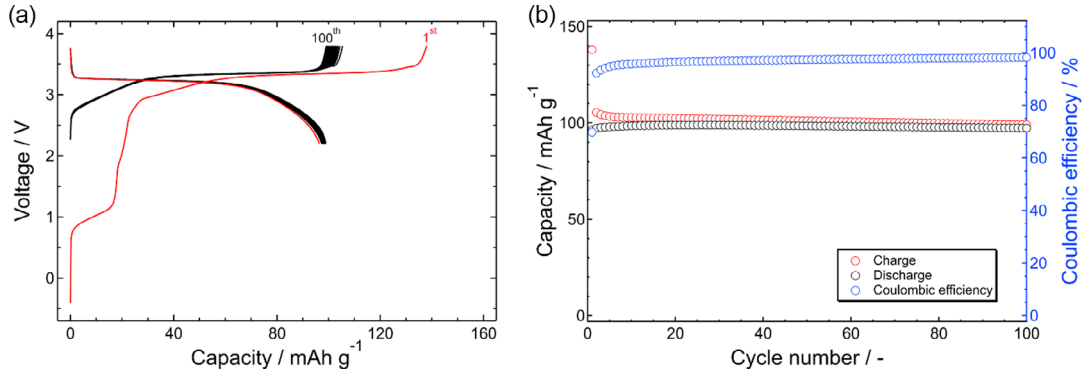

Figure 9. a) Galvanostatic charge–discharge cycling profiles and b) the corresponding Coulombic efficiency of pouch-type [HC || presodiated NVP] full cells.

additional charge plateau at around 1.2 V, attributable to Na^+ extraction from the $Na_4V_2(PO_4)_3$ structure,[26] and a substantially large initial charging capacity was obtained (**Figure 9**). The full cell delivered an initial discharge capacity of 96 mAh g^{-1}, and the deliverable capacities were stabilized at around 100 mAh g^{-1} for subsequent cycles. This observation strongly implies that the stable SEI was formed on the HC electrode by the consumption of extra Na^+ from $Na_4V_2(PO_4)_3$ and most of the reactive Na^+ ions seem to be preserved in the electrodes. Although the mass loading of the above cell is ≈5 mg cm^{-2}, hence optimization with respect to loading amount and N/P ratio is ongoing, the energy density of the present primal full cell with chemically presodiated NVP also reaches ≈100 Wh kg^{-1} (Figure S12 and Table S1, Supporting Information).

3. Conclusion

This work demonstrates how the engineering aspects of batteries, such as the composition of electrodes and N/P ratio, affect the performance of full cells and highlights the importance of adopting positive and negative electrodes with well-balanced capacities to achieve high-energy density practical SIBs. Upon comparative survey, the optimum composition of NVP and HC electrodes with respect to the areal capacity and capacity retention under full-cell operations was proposed. The systematic study on the N/P ratio also clarifies the significant detrimental effect of the consumption of reactive Na^+ by SEI formation on the energy density of full cells. The full cells that adopted either appropriate electrochemical precharging of HC electrodes combined with the well-controlled N/P ratio or chemical presodiation on NVP electrodes achieved a practical energy density of 100 Wh kg^{-1} despite employing primitive electrode materials.

Improvements in capacities and working voltages of electrode materials are straightforward approaches to enhance the energy density of batteries. A practical energy density of 150 Wh kg^{-1} is potentially achievable by adopting prospective positive electrodes with stable capacities of 120 mAh g^{-1} at a working voltage of 3.5 V. In contrast, for the present [HC || NVP] systems, increasing the mass loading of NVP to >19 mg cm^{-2}, which is the same level as positive electrodes of commercialized LIBs, will also lead to an energy density of 150 Wh kg^{-1}. Development in both active materials and techniques of thick electrode fabrication will pave the way for high-energy-density SIB materialization.

4. Experimental Section

Materials: The positive electrode material, $Na_3V_2(PO_4)_3$ (NVP), was procured from Kojundo Chemical Laboratory CO., Ltd., or MTI Corporation and utilized without further treatment. SEM analysis revealed differences in particle morphology between the two NVP samples, with fine irregular and coarse secondary particles observed for the former and the latter, respectively (Figure S1, Supporting Information). Primarily, the finer NVP powder was utilized unless stated otherwise in this study. HC powder, designated KURANODE (Type 1), was generously provided by Kuraray. Prior to use, the HC powder underwent vacuum heating at 200 °C for a minimum of 3 days to eliminate surface-adsorbed moisture. AB (Denka Black, Denka) and a carbon nanotube/fluoropolymer dispersion (CNT; NEOFLON VTD-475 N, Daikin Industries, LTD.) were employed as conductive supports. PVdF powders with varying molecular weights, low (L-PVdF, #1100) and high (H-PVdF, #7500), were obtained from Kureha. The PVdF binder solution for the NVP electrodes was prepared by dissolving a certain amount of predried PVdF powder (≈12 wt%) in anhydrous *N*-methylpyrrolidone (NMP; Kanto Chemical CO., Inc.) under a dry air atmosphere with a controlled dew point of <−76 °C (Dry chamber; Soda Kogyo). For the HC electrodes, a suitable combination of an aqueous dispersion of sodium CMC(CMC2000, Daicel Miraizu) and SBR (TRD104A, ENEOS Material) was utilized as a binder.

Composite NVP and HC electrodes were prepared under dry and ambient atmospheres, respectively, using the appropriate conductive supports and binder. The resulting NVP and HC slurries were applied onto an aluminum current collector and dried at 80 °C for 24 h. The resultant composite sheet electrodes were compressed using a roller pressing machine (Eager Corporation) to enhance electrical conductivity. A standard electrolyte solution of 1 mol dm^{-3} $NaPF_6$/EC-DEC (1:1) (EC: ethylene carbonate, DEC: diethyl carbonate) served as the base electrolyte. Additionally, for comparison, two solutions of 1 mol dm^{-3} $NaPF_6$/diglyme (G2; for electrochemistry, Kanto Chemical CO., Inc.) and 0.5 mol dm^{-3} $Na[B(HFIP)_4]$/EC-DEC (1:1) were prepared. $Na[B(HFIP)_4]$ was synthesized following a reported procedure.[30] The impact of a conventional electrolyte additive, FEC (Merck), on battery performance was also investigated by adding a predetermined amount of FEC to the base electrolyte within an Ar-filled glove box. Polyolefin-based separators were employed for all charge–discharge measurements.

Charge–Discharge Measurements: Charge–discharge cycling tests were conducted using both 2032-type coin cells and pouch-type cells with NVP and HC electrodes. Both half-cell and full-cell configurations were utilized in the tests with coin-type cells. For half cells, Na metal foils (≈200 µm thick) were employed as counter electrodes, while NVP and HC were paired together for full-cell configuration. To minimize contamination from side reactions between Na metal and atmospheric impurities, all half cells were assembled in an Ar-filled glovebox with controlled levels of H_2O and O_2 (<1 ppm). Conversely, both coin and pouch-type full cells were assembled under a dry air atmosphere (dew point ≈−40 °C). The effect of capacity balance between negative and positive electrodes, known as the N/P ratio, was examined by considering the amount of active materials and the practical reversible capacity of NVP (117 mAh g^{-1}) and HC (300 mAh g^{-1}). Electrochemical precharging on HC electrodes was preliminarily carried out by charging the [HC || NVP] coin-type full cells to different depths of charge, followed by disassembling the charged cells, replacing the charged NVP with pristine NVP while leaving other components unchanged, reassembling the cells, and restarting charge–discharge measurements. For the pouch-type cell configuration, the electrochemical precharging was carried out by charging the [HC || NVP for precharging || NVP for cycling] full cells to 100% of depths of charge using NVP for precharging, followed by disassembling the charged cells, removing the NVP for precharging and relevant appurtenance (separator, tab, and tab-lead), reassembling the cells, and restarting charge–discharge measurements with the [precharged HC || NVP for cycling] cells. The configuration of pouch-type cells for electrochemical precharging is illustrated in Figure S2, Supporting Information. Chemically predoped NVP composite cathodes were prepared by soaking the composite in a 0.05 mol dm^{-3} phenazine-Na/G1 solution for 120 s, following literature protocols.[26] Charge–discharge tests were performed at a 1C rate (120 mA g_{NVP}^{-1}) based on the mass of active materials for half-cell configurations and based on the mass of NVP for full-cell configurations, unless otherwise specified.

Characterization: Composite electrodes were observed using SEM (JSM-7800F, JEOL) and subsequently characterized by energy-dispersive X-ray (EDX) spectroscopy. Electrodes for SEM observations were processed using a cross-sectional polisher (CP; IB-09020CP, JEOL) to obtain smooth cross-sectional views. The surface composition of NVP and HC electrodes before and after cycling was examined using XPS(VersaProbe II, ULVACPHI, Japan). All cycled samples were washed with anhydrous DEC to remove residual electrolyte, dried under high vacuum at ambient temperature, placed in an airtight chamber, and transferred for XPS analysis without exposure to air. XPS measurements were conducted with an Al Kα X-ray source under a base pressure of

6.7×10^{-8} Pa. The binding energy of the obtained spectra was calibrated using the C 1*s* peak from sp^2-hybridized carbon at 284.5 eV as a reference.

Supporting Information

Supporting Information is available from the Wiley Online Library or from the author.

Acknowledgements

This work received financial support from the NEXT Center of Innovation Program (COI-NEXT, grant no. JPMJPF2016) of the Japan Science and Technology Agency and a Grant-in-Aid for Scientific Research (KAKENHI, JP21K05263) from the Japan Society for the Promotion of Science. The authors appreciate the support received for SEM observations and XPS measurements at the NIMS Battery Research Platform. T.M. also thanks Prof. Shinichi Komaba and Dr. Kei Kubota for their kind advice on battery fabrication.

Conflict of Interest

The authors declare no conflict of interest.

Author Contributions

T.M.: Conceptualization, data curation, formal analysis, funding acquisition, investigation, project administration, resources, validation, writing–original draft and review and editing. U.T.: Data curation, formal analysis, investigation. S.K.: Dara curation, investigation, formal analysis.

Data Availability Statement

The data that support the findings of this study are available from the corresponding author upon reasonable request.

Keywords

capacity ratio, electrodes, full-cell configurations, sodium-ion batteries

Received: February 24, 2024
Revised: April 16, 2024
Published online: May 19, 2024

[1] United States Geological Survey, *Lithium. Mineral Commodity Summaries*, USGS Publications, Virginia, USA **2023**.
[2] X. Zhang, A. Han, Y. Yang, *J. Mater. Chem. A* **2020**, *8*, 22455.
[3] C. Wang, A. C. Thenuwara, J. Luo, P. P. Shetty, M. T. McDowell, H. Zhu, S. P. Pérez, H. Xiong, G. Hautier, W. Li, *Nat. Commun.* **2022**, *13*, 4934.
[4] U.S. Geological Survey, *Salt. Mineral Commodity Summaries*, USGS Publications, Virginia, USA **2024**.
[5] S. Singh, D. Singh, R. Ahuja, M. Fichtner, P. Barpanda, *J. Mater. Chem. A* **2023**, *11*, 3975.
[6] A. Kamiyama, K. Kubota, D. Igarashi, Y. Youn, Y. Tateyama, H. Ando, K. Gotoh, S. Komaba, *Angew. Chem., Int. Ed.* **2021**, *60*, 5114.
[7] D. M. C. Ould, S. Menkin, H. E. Smith, V. R. Gonzalez, E. Jónsson, C. A. O'Keefe, F. Coowar, J. Barker, A. D. Bond, C. P. Grey, D. S. Wright, *Angew. Chem., Int. Ed.* **2022**, *61*, e202202133.
[8] F. Karcher, M. Uhl, T. Geng, T. Jacob, R. Schuster, *Adv. Energy Mater.* **2023**, *14*, 2302241.
[9] J. Conder, C. Villevieille, J.-M. L. Meins, C. M. Ghimbeu, *ACS Appl. Energy Mater.* **2022**, *5*, 12373.
[10] R.-R. Li, Z. Yang, X.-X. He, X.-H. Liu, H. Zhang, Y. Gao, Y. Qiao, L. Li, S.-L. Chou, *Chem. Commun.* **2021**, *57*, 12406.
[11] C. Müller, Z. Wang, A. Hofmann, P. Stüble, X. L. Théato, J. Klemens, A. Smith, *Batteries Supercaps* **2023**, *6*, e202300322.
[12] A. Rudola, A. J. R. Rennie, R. Heap, S. S. Meysami, A. Lowbridge, F. Mazzali, R. Sayers, C. J. Wright, J. Barker, *J. Mater. Chem. A* **2021**, *9*, 8279.
[13] S. Zhao, R. Qiu, J. Su, F. Li, L. Yantinga, L. Zhenga, Y. Huang, M. Wei, Z. Hong, *J. Power Sources* **2022**, *544*, 231862.
[14] S.-M. Oh, P. Oh, S.-O. Kim, A. Manthiram, *J. Electrochem. Soc.* **2017**, *164*, A321.
[15] H. Chen, M. Ling, L. Hencz, H. Y. Ling, G. Li, Z. Lin, G. Liu, S. Zhang, *Chem. Rev.* **2018**, *118*, 8936.
[16] Q. Meng, Y. Lu, F. Ding, Q. Zhang, L. Chen, Y.-S. Hu, *ACS Energy Lett.* **2019**, *4*, 2608.
[17] X. Dou, I. Hasa, D. Saurel, C. Vaalma, L. Wu, D. Buchholz, D. Bresser, S. Komaba, S. Passerini, *Mater. Today* **2019**, *23*, 87.
[18] A. Ponrouch, D. Monti, A. Boschin, B. Steen, P. Johansson, M. R. Palacín, *J. Mater. Chem. A* **2015**, *3*, 22.
[19] H. Zhao, J. Xu, D. Yin, Y. Du, *Chem. Eur. J.* **2018**, *24*, 18220.
[20] Z. W. Seh, J. Sun, Y. Sun, Y. Cui, *ACS Cent. Sci.* **2015**, *1*, 449.
[21] P. Geysens, V. S. Rangasamy, S. Thayumanasundaram, K. Robeyns, L. V. Meervelt, J.-P. Locquet, J. Fransaer, K. Binnemans, *J. Phys. Chem. B* **2018**, *122*, 275.
[22] S. Terada, T. Mandai, R. Nozawa, K. Yoshida, K. Ueno, S. Tsuzuki, K. Dokko, M. Watanabe, *Phys. Chem. Chem. Phys.* **2014**, *16*, 11737.
[23] S. Komaba, T. Ishikawa, N. Yabuuchi, W. Murata, A. Ito, Y. Ohsawa, *ACS Appl. Mater. Interfaces* **2011**, *3*, 4165.
[24] M. Ma, H. Cai, C. Xu, R. Huang, S. Wang, H. Pan, Y.-S. Hu, *Adv. Funct. Mater.* **2021**, *31*, 2100278.
[25] M. Ue, K. Sakaushi, K. Uosaki, *Mater. Horiz.* **2020**, *7*, 1937.
[26] M. Xu, F. Zhang, Y. Zhang, C. Wu, X. Zhou, X. Ai, J. Qian, *Chem. Sci.* **2023**, *14*, 12570.
[27] K. Zou, W. Deng, P. Cai, X. Deng, B. Wang, C. Liu, J. Li, H. Hou, G. Zou, X. Ji, *Adv. Funct. Mater.* **2021**, *31*, 2005581.
[28] H. Fang, S. Gao, M. Ren, Y. Huang, F. Cheng, J. Chen, F. Li, *Angew. Chem., Int. Ed.* **2023**, *62*, e202214717.
[29] M. Sathiya, J. Thomas, D. Batuk, V. Pimenta, R. Gopalan, J.-M. Tarascon, *Chem. Mater.* **2017**, *29*, 5948.
[30] T. Mandai, H. Naya, M. Hyuma, *J. Phys. Chem. C* **2023**, *127*, 7987.